The Astrophysical Journal, 819:61 (12pp), 2016 March 1 doi:10.3847/0004-637X/819/1/61

A MODEL FOR THE DUST ENVELOPE OF THE SILICATE CARBON STAR IRAS 09425-6040

Kyung-Won Suh
Department of Astronomy and Space Science, Chungbuk National University, Cheongju-City, 28644, Korea; kwsuh@chungbuk.ac.kr
Received 2015 November 2; accepted 2016 January 24; published 2016 February 29

ABSTRACT

IRAS 09425-6040 (I09425) is a silicate carbon star with conspicuous crystalline silicate and water-ice features and emission excesses in the far-infrared and millimeter (mm) wavelength ranges. To understand properties of the dust envelope of I09425, we propose a physical model based on the observations and known properties of asymptotic giant branch stars and dust. We perform radiative transfer model calculations using multiple dust shells and disks with various dust species. We compare the model results with the observed spectral energy distribution (SED) acquired with different telescopes. We find that the physical model for I09425 using multiple shells of carbon and silicate dust and multiple disks of amorphous and crystalline silicates reproduces the observed SED fairly well. This object looks to have detached cold O-rich (silicate and water-ice) dust shells, which could be remnants of the recent chemical transition from O to C and an inner C-rich dust shell. A long-lived thin disk of very large silicate grains can reproduce the emission excess in the mm wavelength band and a recently formed thick disk of crystalline silicates can reproduce the prominent emission features in the spectral range 8–45 μm. The highly crystallized silicates could be recently formed by high temperature annealing due to the last O-rich superwind just before the chemical transition of the central star. I09425 could be a rare object that has the remnants of past O-rich stellar winds in the outer shells as well as in the circumbinary disks.

Key words: circumstellar matter – dust, extinction – infrared: stars – radiative transfer – stars: AGB and post-AGB

1. INTODUCTION

Based on the chemistry of the photosphere and/or the circumstellar envelope, asymptotic giant branch (AGB) stars are generally classified as O-rich (M-type) or C-rich (C-type). Carbon stars are generally believed to be the evolutionary successors of O-rich AGB stars because an O-rich AGB star may become a carbon star when the star goes through C dredge-up processes due to thermal pulses (Iben 1981; Chan & Kwok 1990).

As an AGB star evolves, a thermal pulse due to an internal helium shell flash has been hypothesized as a major cause of an episode of greatly enhanced mass-loss, commonly referred to as a superwind phase (Wood 1990). One thermal pulse every 10^4–10^5 years that endures for a few hundred years is expected (Iben & Renzini 1983; Vassiliadis & Wood 1993). The chemical transition from O to C and superwind, which is induced by a thermal pulse, is known to make major effects on the dust envelopes around AGB stars (e.g., Groenewegen et al. 1995; Suh 2014).

Silicate carbon stars show the characteristics of a carbon star and circumstellar silicate dust features. They were discovered by *IRAS* observations (Little-Marenin 1986; Willems & de Jong 1986). Willems & de Jong (1986) and Chan & Kwok (1991) suggested that silicate carbon stars are objects in transition from O-rich AGB stars to carbon stars. Many of the silicate carbon stars are fairly well fitted with a simple detached silicate dust shell model (e.g., Chan & Kwok 1991). However, this scenario could be unlikely for many objects because the timescale for such a transitional object to be observed as a silicate carbon star is predicted to be short (shorter than about 400 years; Kwon & Suh 2014). So far, about 29 silicate carbon stars have been identified in our Galaxy (Kwon & Suh 2014).

Morris (1987) and Lloyd Evans (1990) suggested that a silicate carbon star is a binary system that has a primary carbon star and a low-luminosity companion. When the primary is still an O-rich AGB star, O-rich material is supposed to be used to form a relatively long-lived disk of silicate dust. The disk may serve as a reservoir of O-rich dust even after the primary star evolves into a carbon star. This scenario is believed to be promising (e.g., Yamamura et al. 2000; Ohnaka et al. 2008).

IRAS 09425-6040 (hereafter, I09425) is a silicate carbon star with conspicuous crystalline silicate and water-ice features and emission excesses in the far-infrared (FIR) and millimeter (mm) wavelength ranges. For I09425, Molster et al. (2001) identified various molecular and dust bands and proposed that crystalline silicates are located in a long-lived disk using a spherically symmetric dust shell model. The purpose of this paper is to study detailed properties of multiple dust components of the circumstellar envelope by using a more sophisticated theoretical model for I09425. We perform radiative transfer model calculations for various possible combinations of dust shells and disks with various dust species. We compare the resulting spectrum with the observed spectral energy distribution (SED) described by the *Infrared Astronomical Satellite* (*IRAS*) Point Source Catalog (PSC), *Infrared Space Observatory* (*ISO*), *AKARI*, and Two-Micron All-sky Survey (2MASS) data.

2. OBSERVATIONS OF I09425

In Figure 1, we show the observed SED compared with the theoretical model results (see Section 6). We plot the observed SED described by the *ISO*, *AKARI*, and 2*MASS* data. We also plot the *IRAS* PSC and Low Resolution Spectrograph (LRS; $\lambda = 8$–$22\ \mu$m) data. We cross-identify the *AKARI* and 2MASS counterparts by finding the nearest source from the position information in the *IRAS* PSC. We use the *AKARI* PSC data in two bands and bright-source catalog (BSC) data in four bands. The NIR photometric data obtained by García-Lario et al. (1997) are also displayed. We plot the flux at 1.3 mm observed by Molster et al. (2001) who reported a continuum emission excess. Table 1 summarizes the observed fluxes of I09425.

This object was observed by the *ISO* Short Wavelength Spectrometer (SWS; $\lambda = 2.4$–$45.4\ \mu$m) two times. Molster

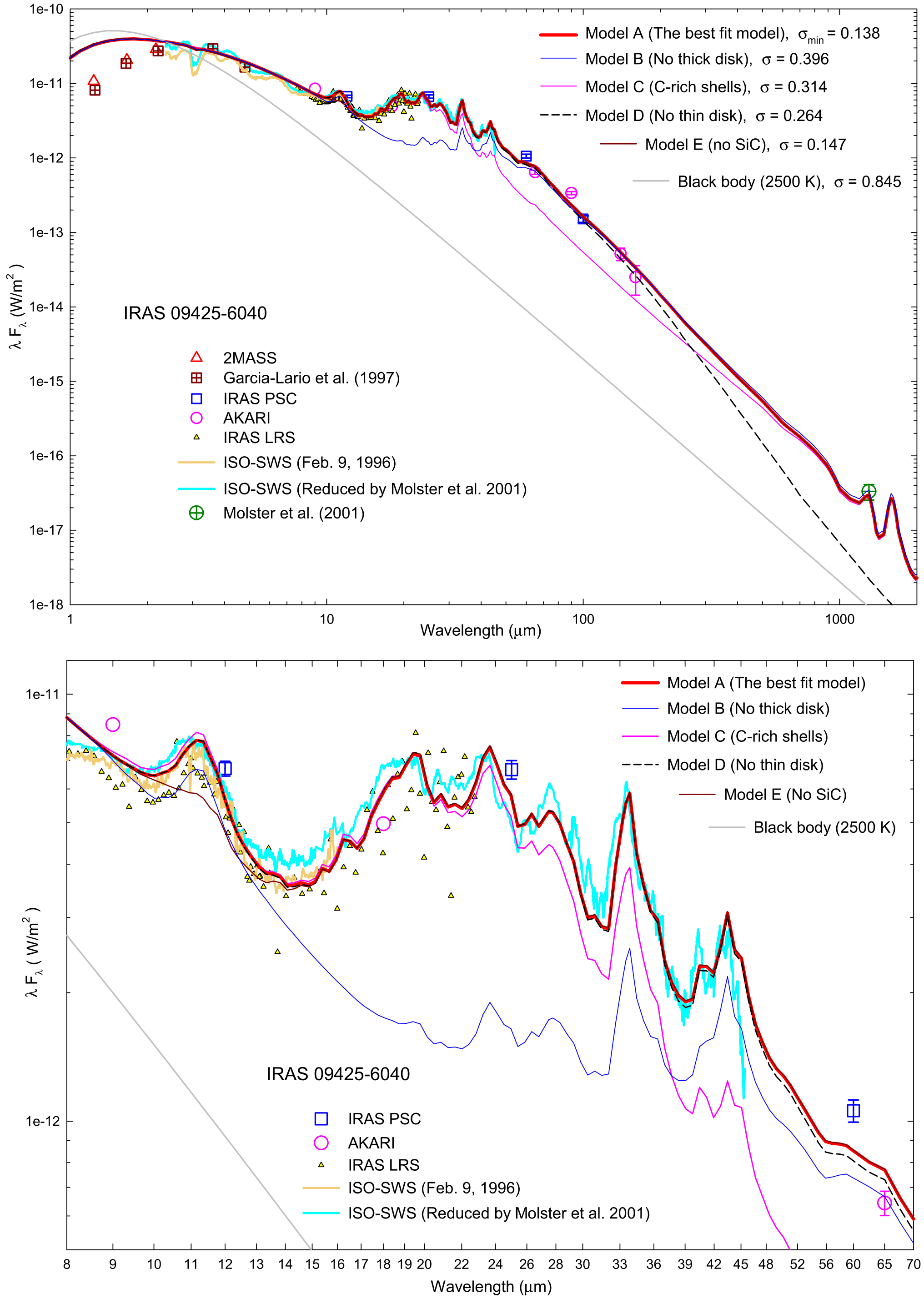

Figure 1. SED of IRAS 09425-6040 compared with theoretical models (see Section 6). For all of the theoretical models, the distance and viewing angle are assumed to 1.8 kpc and 75°, respectively. See Equation (8) for the definition of σ.

et al. (2001) analyzed the *ISO* spectra and identified various molecular and dust bands. I09425 shows the emission feature at 11.3 μm due to SiC dust and conspicuous emission features of crystalline silicates (forsterite features: 19.5, 23.5, 27.5, and 33.5 μm; enstatite features: 40.8 and 43.4 μm) and water-ice (at 44 μm) in the wavelength range 8–45.4 μm. In Figure 1, we plot the *ISO* SWS data reduced by Molster et al. (2001). We also plot the original *ISO* SWS spectrum obtained on 1996 February 9.

Searches for the molecular maser emissions from OH (Galt et al. 1989), H_2O (Zuckerman & Lo 1987), and SiO (Jiang et al. 1996) all failed. There is not yet any direct observational evidence of binarity or a disk for I09425.

The distance to I09425 is uncertain. Molster et al. (2001) estimated it to be 1.3 kpc assuming that the luminosity is $6.5 \times 10^3\,L_\odot$. García-Hernández et al. (2006) estimated the distance to be 2.7 kpc, which is the distance to the Carina complex and derived the luminosity of $1.25 \times 10^4\,L_\odot$. In this

Table 1
Observed Fluxes of I09425

Telescope	Wavelength (μm)	Observed (Jy)	Date	Reference
IRAS PSC	12, 25, 60, 100	26.8 ± 1.1, 55.5 ± 2.8, 21.2 ± 1.3, 5.06 ± 0.51	1983	...
IRAS LRS	8–22	...	1983	...
ESO 1 m	1.25, 1.65, 2.2, 3.6, 4.8	3.39, 10.2, 20.1, 35.2, 26.5	1990 May 6–11	García-Lario et al. (1997)
ISO SWS	2.4–45.4	...	1996 Feb 9	...
ISO SWS	2.4–45.4	...	1996 Jul 27	Reduced by Molster et al. (2001)
SEST	1300	14.4 ± 3.4 mJy	...	Molster et al. (2001)
2*MASS*	1.25, 1.65, 2.17	4.42 ± 0.08, 11.5 ± 0.60, 20.7 ± 4.8	2000 Jan 8	Cutri et al. (2003)
AKARI PSC	9, 18	25.5 ± 1.3, 29.9 ± 2.5	2006–2007	Murakami et al. (2007)
AKARI BSC	65, 90, 140, 160	14.0 ± 0.91, 10.1 ± 0.46, 2.41 ± 0.45, 1.34 ± 0.57	2006–2007	Murakami et al. (2007)

work, we assume that the luminosity is $7 \times 10^3 L_\odot$ and the distance is estimated to be 1.8 kpc (see Section 6.1).

3. THEORETICAL MODELS FOR I09425

We propose a physical model for the dust envelope of I09425 based on the observations of the object and known properties of silicate carbon stars and dust.

3.1. Binarity and Circumstellar Disks

Even though there is no direct observational evidence of binarity or a circumstellar disk for I09425 yet, there are many reasons to believe that most silicate carbon stars are binary systems that have circumstellar disks (see Section 1). Molster et al. (2001) modeled I09425 assuming spherical symmetry and deduced that the object is probably a binary system and there could be a dust disk in the envelope. They suggested that the emission excess at 1.3 mm is likely to be produced by very large dust grains in the disk. It is difficult to imagine that the size of silicate grains can grow up to 300 μm in the outer expanding dust shells. Because circumstellar disks are believed to be suitable for growth of dust grains (e.g., Sauter & Wolf 2011), we expect that the size of dust grains in a long-lived disk can be very large. Therefore, we expect that the emission excess at 1.3 mm could be produced by very large silicate grains in the disk (see Sections 5.2 and 6.4 for details).

3.2. The Chemical Transition from O to C

For I09425, there is some observational evidence of a recent chemical transition from O to C. García-Hernández et al. (2006) derived the abundance ratios $C/O = 1.01$, $^{12}C/^{13}C = 15 \pm 6$, and $\log(Li/H) + 12 \sim 0.7 \pm 0.4$, which are typical characteristics of J-type carbon stars (e.g., Chen et al. 2007). García-Hernández et al. (2006) argued that the detection of Li and presence of C-rich gas-phase molecules in the *ISO* spectrum of the central star suggest that the chemical transition was relatively recent because Li has not been destroyed and there has been no time to form more complex molecules such as polycyclic aromatic hydrocarbons (PAHs). They expected that the previously expelled O-rich material may still remain in the outer shell.

3.3. Origin of Crystalline Silicates

Fabian et al. (2000) investigated the thermal evolution of amorphous silicate grains and they found that annealing at a temperature of 1000 K transformed amorphous silicate grains to crystalline ones in relatively short timescales (one to several days). For high mass-loss rate AGB stars, the annealing crystallization process can be effective because the dust formation temperature is about 1000 K and the inner region of the outflowing dust shell is hot (1000–900 K) during an extended period of time (several hundred days; Suh 2002). Suh (2002) found that dust shell models with about 10%–20% of crystalline silicates can reproduce the observed crystalline silicate features for high mass-loss rate O-rich AGB stars.

The dust formation temperature, which is about 1000 K for high mass-loss rate AGB stars, would be higher in a superwind phase because a higher mass-loss rate implies a higher dust formation temperature (1300–1000 K; see Suh 2004). The superwind may provide a better condition for crystallizing silicate dust by efficient high temperature annealing in the inner region of the dust shell.

For I09425, crystalline silicates could be formed by high-temperature annealing due to the superwind which is induced by the last thermal pulse as an O-rich star in the chemical transition phase. The superwind could produce a density enhanced O-rich dust shell with crystalline silicates (a superwind dust shell). Suh (1997) showed that a tenfold increase in the density of a dust shell can reasonably reproduce the effects of a superwind for carbon stars. In a binary system, the O-rich superwind could form a stationary disk of crystalline silicate dust as well as the expanding superwind dust shell.

3.4. Water-ice Features

It has been known that some of the high mass-loss rate OH/IR stars show water-ice features. Justtanont et al. (2006) found that the water-ice absorption feature at 3.1 μm is stronger for OH/IR stars with higher mass-loss rates. For some OH/IR stars observed by *ISO*, Suh & Kwon (2013) reproduced their water-ice absorption features at 3.1 and 11.5 μm and emission features at 44 and 62 μm by using a dust shell model of water-ice coated silicates. For the OH/IR stars with higher mass-loss rates, the condition for water-ice formation would be better because the thicker dust shell may effectively shield the water-ice from the stellar radiation.

If the outer radius of a disk is smaller than the radius where water-ice mantles form, the circumstellar disk may not provide good conditions for forming water-ice mantles because the disk is likely to be warmer and more exposed to the stellar radiation for longer timescales. In this case, the detection of water-ice in I09425 may indicate the existence of both O-rich (water-ice) and C-rich dust (SiC) in the expanding dust shells.

3.5. A Physical Model for I09425

Considering the observational characteristics of I09425 in various respects as discussed above, we propose a theoretical model for the object using multiple dust shells and disks around a carbon star.

We assume that the object is a binary system with a carbon star and an unseen companion. For radiative transfer model calculations, we may ignore the contribution of the unseen companion if we assume that the luminosity contrast between the primary star and its companion is enormous.

We assume that the chemical transition from O to C occurred recently for the carbon star. There could be a superwind, which is due to the last thermal pulse as an O-rich star in the chemical transition phase.

We assume that the object has a reservoir of dust in a disk shape. The disk may serve as a reservoir of O-rich stellar winds even after the star evolves into a carbon star. There could be O-rich dust grains in the outer expanding dust shell as well as in the disk because the chemical transition is recent.

There could be detached O-rich dust (silicate and water-ice) shells, which are remnants of the chemical transition from O to C, and an inner C-rich dust shell. The inner detached O-rich dust shell could have a density enhancement due to the last O-rich superwind. In the superwind dust shell, silicate grains could be more efficiently crystallized by high-temperature annealing during the superwind phase (see Section 3.3).

In addition to the relatively long-lived thin disk of large silicate dust grains which was formed when the primary was an O-rich AGB star, there could be another dust disk that recently formed from the last O-rich superwind in the chemical transition phase. The superwind could be able to produce a new thicker disk with highly crystallized silicate dust.

4. RADIATIVE TRANSFER MODEL CALCULATIONS

To test the physical model for the dust envelope of I09425 (see Section 3), we perform radiative transfer model calculations to be compared with the observations. In this work, we use the radiative transfer code RADMC-3D (http://www.ita.uni-heidelberg.de/~dullemond/software/radmc-3d/) to calculate model SEDs for the dust envelope of the silicate carbon star. RADMC-3D is a software package for astrophysical radiative transfer calculations in arbitrary geometries. It is mainly written for continuum radiative transfer in dusty media based on the Monte Carlo simulation method of Bjorkman & Wood (2001).

In this work, we consider multiple spherically symmetric dust shells and multiple axi-symmetric dust disks around a single star. Dust species in each dust shell or disk may have its own density structure. For given density structures, the code calculates the dust temperature and scattering source function at every geometric point in the model. At each wavelength, the code integrates the intensity inside synthetic observing apertures to calculate the model SED.

4.1. Spherically Symmetric Dust Shells

For pulsating AGB stars, the overall continuous density distribution is believed to be maintained for a timescale larger than the pulsation period (e.g., Suh 2004). But there could be an abrupt change in the mass-loss rate because of a superwind induced by a thermal pulse (e.g., Suh 1997).

We consider multiple dust shells that are spherically symmetric around a central star. We assume that the dust density distribution is continuous ($\rho \propto r^{-2}$) from the inner radius ($R_{\rm in}$) to the outer radius ($R_{\rm out}$) for each dust shell. However, each dust shell has its own density enhancement factor (β) relative to the overall continuous density distribution.

For each dust shell, the dust density is given by

$$\rho(r) = \rho_{\rm in}(R_{\rm in}/r)^2, \tag{1}$$

where $\rho_{\rm in}$ is the dust density at $R_{\rm in}$. $\rho_{\rm in}$ is given by

$$\rho_{\rm in} = \beta\rho_0(R_0/R_{\rm in})^2, \tag{2}$$

where β is the density enhancement factor of the dust shell and ρ_0 is the dust density at R_0 which is taken to be 10 au. The dust mass-loss rate ($\dot{M}_{\rm dust}$) is given by

$$\dot{M}_{\rm dust} = 4\pi R_{\rm in}^2\rho_{\rm in}V_{\rm exp} = 4\pi\beta\rho_0 R_0^2 V_{\rm exp}, \tag{3}$$

where $V_{\rm exp}$ is the dust shell expansion velocity. $\dot{M}_{\rm dust}$ and $V_{\rm exp}$ are assumed to be constant for each dust shell.

4.2. Axi-symmetric Dust Disks

We consider multiple axi-symmetric dust disks around a central star. Each dust disk has its density distribution from the inner radius ($R_{\rm in}$) to the outer radius ($R_{\rm out}$). For the dust density distribution of the disks, we use the distribution function presented by Juhász et al. (2009) for moderately flared and flat disks.

For each disk, the dust density is given by

$$\rho(r, z) = \frac{\Sigma(r)}{\sqrt{2\pi}H_p(r)}\exp\left[-0.5\left(\frac{z}{H_p(r)}\right)^2\right], \tag{4}$$

where r is the radial distance from the star, z is the height above the disk plane, Σ is the surface density in the disk, and $H_p(r)$ is the pressure scale height in the disk. The pressure scale height is given by $H_p(r) = c_s/\Omega_K$, where c_s and $\Omega_K = \sqrt{GM/r^3}$ denote the speed of sound and the local Kepler frequency, respectively. The surface density of dust in the disk as a function of r is given by:

$$\Sigma(r) = \Sigma_0(r/R_0)^{-p}, \tag{5}$$

where Σ_0 is the density at R_0 which is a fixed radius (800 au) and p is the power-law index. A similar power-law equation holds for the pressure scale height (Kenyon & Hartmann 1987):

$$\frac{H_p(r)}{r} = h_0\left(\frac{r}{R_0}\right)^{\alpha}, \tag{6}$$

where α is the flaring index and h_0 is given by

$$h_0 = \frac{H_p(R_0)}{R_0}. \tag{7}$$

Disks with large flaring indices indicate rapidly rising curves, while non-flaring disks will show flat curves.

In this work, we assume that the disk is moderately flared ($\alpha = 2/7$) and $\Sigma(r) \propto r^{-1}$ ($p = 1$). We use adjustable h_0 to test various thicknesses of the disk. A larger h_0 makes a thicker disk in the z direction (see Section 6.4).

5. DUST PROPERTIES

5.1. Formation and Growth

In the circumstellar envelopes around typical AGB stars, the dust condensation temperature is believed to be about 1000 K and the final grain radius is about 0.1 μm and is reached within

Table 2
Dust Opacity Functions Used in This Work

Acronym	Radius (μm)	Description	Density (g cm^{-3})	Usage[a]	Reference
AMC	0.1	amorphous carbon	2.0	C-rich shell	Suh (2000)
SiC	0.1	α-SiC	3.26	C-rich shell	Pégourié (1988)
SIL	0.1	amorphous silicate	3.3	O-rich Shell	Suh (1999; cold)
FK	…	crystalline forsterite	3.27	No	Koike et al. (2003)
EK	…	crystalline enstatite	3.27	No	Chihara et al. (2002)
SFE50[b]	…	crystalline silicate	3.285	O-rich shell and disk	a simple mixture of MACs
ICE	0.1	crystalline water-ice	0.92	No	Bertie et al. (1969)
SWC	0.1, 0.2	SIL core, ICE mantle	1.22	O-rich shell	SIL and ICE
S300	300	large amorphous silicate	3.3	O-rich disk	Suh (1999; cold)

Notes.
[a] Usage in the theoretical dust shell or disk model (see Table 3),
[b] SFE50 = SIL(50%) + FK(25%) + EK(25%).

one week (Suh et al. 1990). We assume that dust formation (or growth) is instantaneous because the timescales are believed to be much shorter than the dynamic timescales for AGB stars (e.g., Suh 1999). The dust formation temperature looks to be higher for the AGB stars with higher mass-loss rates (see Suh 2004). The dust size distribution for AGB stars could be a Gaussian distribution rather than a power law which is more relevant to interstellar dust (e.g., Kozasa et al. 1984; Suh 2014).

The dust opacity function for a Gaussian size distribution with a mean radius (e.g., 0.1 μm) with some dispersion does not show major differences from the opacity for the uniform dust size. For simplicity, we assume that all dust grains are spherical with a uniform radius of 0.1 μm except for water-ice coated mantles and very large spherical silicate dust grains which are useful for the long-lived dust disk.

5.2. Dust Opacity

The spectra of O-rich AGB stars (M-type Miras and OH/IR stars) suggest the presence of amorphous and crystalline silicate dust grains in the circumstellar envelopes around them (Jones & Merrill 1976; Suh 1999, 2002). For carbon stars, amorphous carbon (AMC) and SiC dust grains are believed to be the major dust components for their IR spectra (e.g., Suh 2000).

In this work, we use AMC, SiC, amorphous silicate, crystalline water-ice, crystalline forsterite, and crystalline enstatite for the dust opacity (see Table 2). We use the optical constants of AMC dust derived by Suh (2000) and optical constants of SiC derived by Pégourié (1988). For amorphous silicates (SIL), we use the optical constants derived by Suh (1999) for cold silicate dust. For crystalline H_2O ice (ICE), we use the optical constants obtained by Bertie et al. (1969). For AMC, SiC, SIL, and ICE, we assume that the spherical grains have a uniform radius of 0.1 μm.

We use mass absorption coefficients (MACs) of the synthetic forsterite (FK) obtained by Koike et al. (2003) for crystalline forsterite. For crystalline enstatite, we use MACs of the clino-enstatite (EK) obtained by Chihara et al. (2002). Because the formation temperatures for crystalline and amorphous silicates are almost the same, we may use a simple mixture as a single dust component. For the crystalline silicate dust component (SFE50), we use a simple mixture of amorphous silicates (SIL: 50%) and crystalline silicates (FK: 25%; EK: 25%).

We assume that water-ice condenses onto existing cores of silicate (SIL or SFE50) grains. For water-ice, we use coated spherical grains (SWC) of silicate (SIL) cores (0.1 μm) coated with water-ice (ICE) mantles (outer radius: 0.2 μm). Because optical constants of the crystalline silicates in a wide wavelength range are not known well, we use the optical constants of SIL for all of the silicate cores coated by water-ice mantles. The water-ice content (by mass) of the SWC grains is about 66%.

We calculate the mass extinction (absorption and scattering) coefficients using Mie theory (Bohren & Huffman 1983) from the optical constants given in the references for the four dust species (AMC, SiC, SIL, and SWC). For SFE50, we use the MACs which are weighted averages of the three sets of the MAC data (SIL: 50%; FK: 25%; EK: 25%) and the mass scattering coefficients of SIL. A similar scheme was used in Suh (2002) and Suh & Kwon (2013). The upper panel of Figure 2 shows the opacity functions (MACs) for the dust species.

The lower panel of Figure 2 shows the MACs for very large spherical silicate dust grains with various sizes. For the very large grains, we use a new Mie code developed by Wolf & Voshchinnikov (2004) to calculate the extinction coefficients from the optical constants derived by Suh (1999) for cold silicate dust. After using various dust sizes (up to 1000 μm) for model calculations, we have found that the spherical silicate grains with a uniform radius of 300 μm (S300) in a thin disk produce the most similar emission excess at 1.3 mm for I09425 (see Figure 1 and Section 6).

Table 2 lists the dust species used in this work. For all of the model calculations presented in this paper, the dust scattering is assumed to be isotropic.

6. MODEL RESULTS AND COMPARISON WITH OBSERVATIONS

Based on the proposed physical model for I09425 (see Section 3), we perform model calculations for various possible combinations of dust shells and disks with different dust species (see Sections 4 and 5). Considering known properties of silicate carbon stars and circumstellar dust envelopes around AGB stars (e.g., Kwon & Suh 2014; Suh 2014), the ranges of the model parameters for the proposed physical model (see Section 3) could be constrained. The suggested theoretical predictions can be tested by comparison of the model results with the observations until we find the best-fit model for the object.

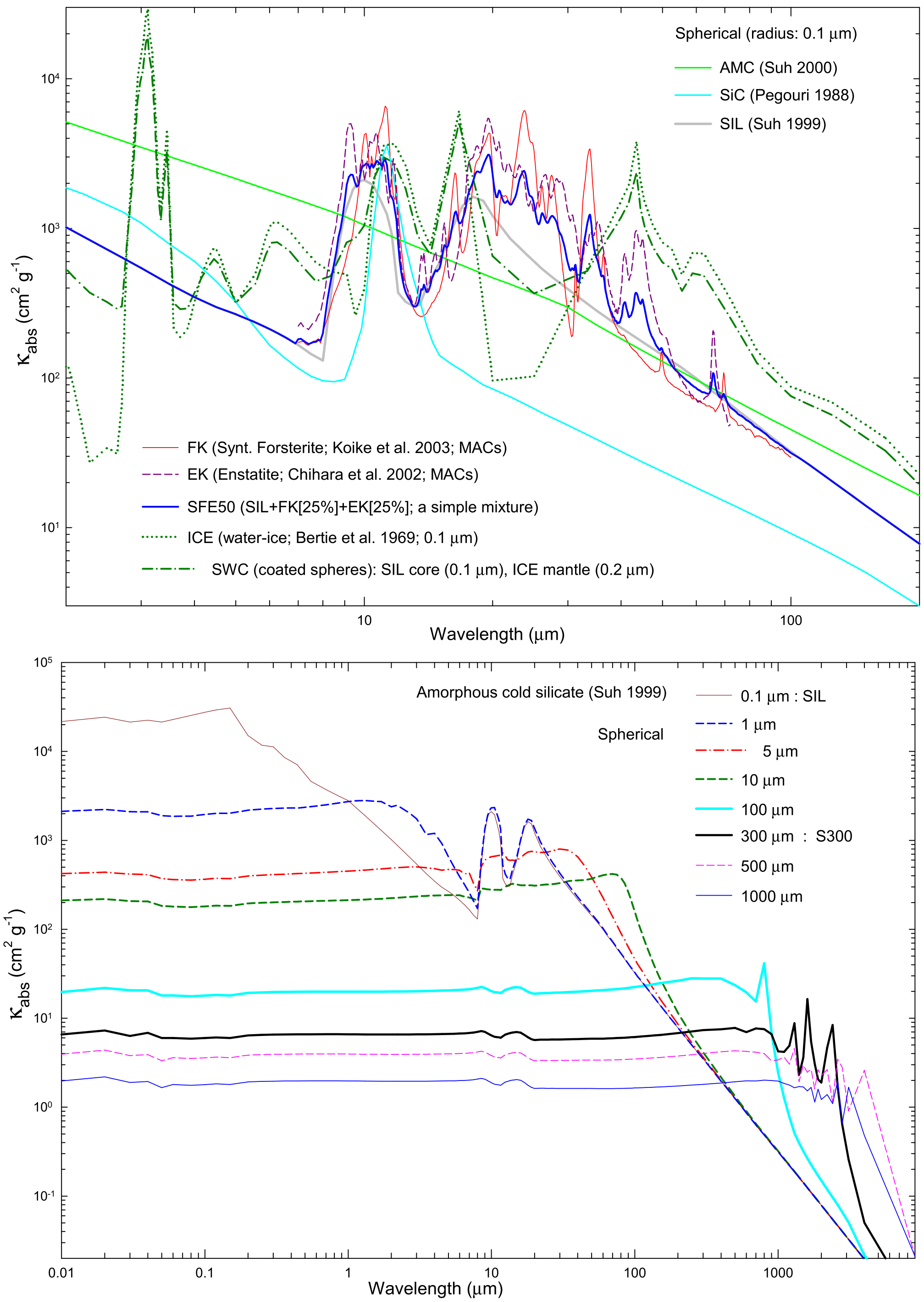

Figure 2. Mass absorption coefficients (MACs) for the dust species used in this work (see Table 2).

The best-fit model shows the smallest σ value, which measures the deviations of the model SED from the observed SED in a wide wavelength range. σ is defined by

$$\sigma = \sqrt{\sum_{i=1}^{n} w_i \left(\frac{O_i - C_i}{O_i}\right)^2 \Big/ \sum_{i=1}^{n} w_i}, \tag{8}$$

where O_i is the observed flux in the wavelength range, w_i is the weight function of O_i, and C_i is the calculated model flux. Note that the deviation is normalized to the observed flux level. w_i is usually taken to be 1.

6.1. The Best Fit Model

In Figure 1, we compare the model results with the observed SED for I09425. This figure also shows the σ values for the theoretical models which were measured in the wavelength range 2.4–1300 μm using the observational data from the *ISO* spectrum reduced by Molster et al. (2001), *IRAS* PSC, *AKARI*, and SEST (see Table 1). We present the model SED of the best fit theoretical model (Model A), which shows the minimum σ value ($\sigma_{\rm min} = 0.138$), using six dust shell components and double dust disk components. We also show the model SEDs of four alternative models (Models B to E) to verify the

Table 3
The Model Parameters for Multiple Disks and Shells

Components	Parameters	Model A The best fit			Model B No thick disk		
Shells	Dust[a]	AMC, SiC	SFE50, SWC	SIL, SWC	AMC, SiC	SFE50, SWC	SIL, SWC
Input	$R_{\rm in}$ (au)	10, 10	3000, 3000	4000, 4000	10, 10	3000, 3000	4000, 4000
	$R_{\rm out}$ (au)	3000, 3000	4000, 4000	15000, 15000	3000, 3000	4000, 4000	15000, 15000
	ρ_0(10 au) (g cm^{-3})	3.0E-19			3.0E-19		
	β	0.9, 0.2	290, 50	18, 16	0.9, 0.2	290, 50	18, 16
Derived	$M_{\rm dust}$ ($M_\odot$)	1.7E-6, 3.8E-7	1.9E-4, 3.2E-5	1.3E-4, 1.1E-4	1.7E-6, 3.8E-7	1.9E-4, 3.2E-5	1.3E-4, 1.1E-4
	τ_{10}	4.1E-2, 2.5E-3	2.4E-2, 1.7E-3	3.0E-3, 1.3E-3	4.1E-2, 2.5E-3	2.4E-2, 1.7E-3	3.0E-3, 1.3E-3
Output	T_c (K)	1059, 1118	54, 52	51, 47	1054, 1110	66, 60	64, 54
Disks	Dust[a]	S300	SFE50		S300		
Input	$R_{\rm in}$ (au)	150	150		150		
	$R_{\rm out}$ (au)	1000	1000		1000		
	Σ_0(800 au) (g cm^{-2})	4.0E-4	4.4E-5		4.0E-4		
	h_0	0.01	0.1		0.01		
Derived	$M_{\rm dust}$ ($M_\odot$)	1.5E-4	2.0E-5		1.5E-4		
Output	$T_{\rm in,disk}$ (K)	216	221		207		
Components	Parameters	Model C C-rich shells			Model D No thin disk		
Shells	Dust[a]	AMC, SiC	AMC, SiC	AMC, SiC	AMC, SiC	SFE50, SWC	SIL, SWC
Input	$R_{\rm in}$ (au)	10, 10	3000, 3000	4000, 4000	10, 10	3000, 3000	4000, 4000
	$R_{\rm out}$ (au)	3000, 3000	4000, 4000	15000, 15000	3000, 3000	4000, 4000	15000, 15000
	ρ_0(10 au) (g cm^{-3})	3.0E-19			3.0E-19		
	β	0.9, 0.2	9, 2	0.9, 0.2	0.9, 0.2	290, 50	18, 16
Derived	$M_{\rm dust}$ ($M_\odot$)	1.7E-6, 3.8E-7	5.8E-6, 1.3E-6	6.3E-6, 1.4E-6	1.7E-6, 3.8E-7	1.9E-4, 3.2E-5	1.3E-4, 1.1E-4
	τ_{10}	4.1E-2, 2.5E-3	3.0E-4, 1.8E-5	7.4E-5, 4.5E-6	4.1E-2, 2.5E-3	2.4E-2, 1.7E-3	3.0E-3, 1.3E-3
Output	T_c (K)	1058, 1117	74, 81	67, 73	1057, 1115	56, 53	53, 48
Disks	Dust[a]	S300	SFE50		SFE50		
Input	$R_{\rm in}$ (au)	150	150		150		
	$R_{\rm out}$ (au)	1000	1000		1000		
	Σ_0(800 au) (g cm^{-2})	4.0E-4	4.4E-5		4.4E-5		
	h_0	0.01	0.1		0.1		
Derived	$M_{\rm dust}$ ($M_\odot$)	1.5E-4	2.0E-5		2.0E-5		
Output	$T_{\rm in,disk}$ (K)	215	220		221		

Note.
[a] See Table 2.

contributions of some important dust components. The model SED is sensitively dependent on the viewing angle i ($i = 90°$ for the edge-on view). We use $i = 75°$ (see Section 7.4) for all of the model SEDs displayed in Figure 1.

Table 3 lists the model parameters for the best fit model (Model A) and three alternative models (Models B to D). For the dust density distribution, the meanings of all the input parameters are explained in Section 4. We use four adjustable input parameters for a dust disk and another four parameters for a dust shell. For each dust component, some useful parameters derived from the input parameters are also listed in Table 3. $M_{\rm dust}$ is the total mass of dust in the component. For a dust shell model, τ_{10} is the dust optical depth at 10 μm. $V_{\rm exp}$ for CO gas was measured to be 10 km s^{-1} (Loup et al. 1993) for I09425. Because the dust expansion velocity could be two times larger than the gas expansion velocity (e.g., Lagadec et al. 2012), we assume that $V_{\rm exp} = 15 \pm 5$ km s^{-1} for all dust shell components. The dust mass-loss rate (see Equation (3)) for all dust shells is given by: $\dot{M}_{\rm dust}\,(M_\odot\ {\rm yr}^{-1}) = (2.0 \pm 0.7) \times 10^{-9} \times \beta$.

Some important output parameters (T_c and $T_{\rm in,disk}$) are listed in Table 3. For a dust shell model, T_c is the dust temperature at $R_{\rm in}$. Even though T_c is not necessarily the same as the dust formation temperature depending on the physical condition of a pulsating AGB star (see Suh 2004), it may be roughly regarded as the dust formation temperature for the innermost dust shell. For a dust disk model, $T_{\rm in,disk}$ is the dust temperature at $R_{\rm in}$.

For Model A, we estimate the uncertainty of a model parameter, which is the range of the parameter that makes a similar σ value ($\sigma < 1.1 \times \sigma_{\rm min}$) in the wavelength range 2.4–1300 μm (see Figure 1) assuming that the rest of the model parameters are fixed. For the O-rich dust shells and disks, the uncertainties of the inner radius, outer radius, and dust mass (or dust density) are about 10%, 25%, and 20%, respectively. For the C-rich dust shell whose density (or β) is relatively lower, the uncertainties of the inner radius, outer radius, and dust mass are about 30%, 60%, and 45%, respectively.

We present the numerical uncertainties of the major model parameters for the dust components in Model A (see Table 3).

For the C-rich dust shell, the inner and outer radii are 10 ± 3 and 3000 ± 2000 au, respectively. For the O-rich dust shell, the inner and outer radii are, respectively, 3000 ± 300 and $15{,}000 \pm 4000$ au. The total dust masses of the C-rich and O-rich dust shells are $(2.1 \pm 0.9) \times 10^{-6}$ and $(4.6 \pm 0.9) \times 10^{-4}\, M_\odot$, respectively. For the O-rich dust disk, the inner and outer radii are, respectively, 150 ± 15 and 1000 ± 250 au and the disk contains the total dust mass of $(1.7 \pm 0.3) \times 10^{-4}\, M_\odot$. We may also estimate the total mass for gas and dust by assuming that the dust-to-gas ratio (δ) is 0.01 (e.g., Suh 2014).

For the central star, we assume that the luminosity (L_*) is $7 \times 10^3\, L_\odot$ and the stellar blackbody temperature (T_*) is 2500 K, which are typical for a carbon star. The estimated distance from the best fit theoretical model is 1.8 kpc.

6.2. Overall SED Comparison

The best-fit model (Model A) can reproduce the overall observed SED fairly well. It uses the six dust shell components: two components of the C-rich dust shell ($r \approx$ 10–3000 au; AMC, SiC), two components of the outer O-rich dust shell with a density enhancement ($r \approx$ 3000–4000 au; SFE50, SWC), and two components of the outermost O-rich dust shell ($r \approx$ 4000–15,000 au; SIL, SWC). It also uses two dust disk components in a radial region ($r \approx$ 150–1000 au): a thin disk with large silicate grains (S300) and a thick disk with crystalline silicates (SFE50).

Highly (~50%) crystallized silicate grains (SFE50) in the outer shell and thick disk reproduce forsterite features at 19.5, 23.5, 27.5, and 33.5 μm and enstatite features at 40.8 and 43.4 μm. As reported by Molster et al. (2001), we also find that higher (~75%) crystallization is required to reproduce the observed SED when we use the opacity functions of crystalline silicates obtained by Jäger et al. (1998). This is because the opacity functions of the crystalline silicates used in this paper (FK and EK; see Table 1) show more conspicuous crystalline features than the ones obtained by Jäger et al. (1998). For I09425, the FK and EK can reproduce the crystalline silicate features better.

Water-ice grains (SWC) reproduce the evident emission feature at 44 μm and weak emission feature at 62 μm fairly well (see Figure 1). The 44 μm water-ice feature is much stronger than the enstatite features at 40.8 and 43.4 μm (see Figure 2). Because the water-ice shell is located outside ($r \gtrsim 3000$), the water-ice grains produce very weak absorption at 3.1 μm (see Suh & Kwon 2013). The deep absorption feature of the observed SED at around 3.1 μm is mainly due to C-rich gas-phase molecules (C_2H_2 and HCN; Molster et al. 2001).

Figure 3 shows dust density and temperature distributions of the six dust shell components and two dust disk components in the direction of the disk plane ($z = 0$) for Model A.

6.3. Multiple Dust Shells and a Superwind

Model A uses detached O-rich dust ($r \approx$ 3000–15,000 au) shells. The O-rich dust shell with a density enhancement (the superwind shell; $r \approx$ 3000–4000 au; SFE50, SWC; $\beta = 290,\ 50$; $T_c = 54,\ 52$ K) and outermost dust shell ($r \approx$ 4000–15,000 au; SIL, SWC; $\beta = 18,\ 16$; $T_c = 51,\ 47$ K) reproduce the FIR excess ($\lambda =$ 20–700 μm). The tenfold increase in the density for the superwind shell of highly (~50%) crystallized silicates (SFE50), which could be due to the last O-rich superwind (see Sections 3.3 and 3.5). The dust mass-loss rate ($\dot{M}_{\rm dust}$) of the superwind shell is $(6.8 \pm 2) \times 10^{-7}\, M_\odot\,{\rm yr}^{-1}$ which is ten times larger than the one for the outermost shell.

The inner C-rich dust shell ($r \approx$ 10–3000 au; AMC, SiC; $\beta = 0.9,\ 0.2$; $T_c = 1059,\ 1118$ K) contributes to reproducing the MIR range ($\lambda =$ 5–20 μm). Note that the dust density enhancement factor β (or the dust mass-loss rate; see Equation (3)) for the C-rich dust shell is 31 times smaller than that for the outermost O-rich dust shell (see Table 2). The SiC component ($\tau_{10} = 0.0025$) produces the evident 11.3 μm feature. The SiC content (by mass) of the C-rich dust shell is about 18%. The alternative Model E, which does not use SiC for the C-rich dust shell, demonstrates that the emission feature at 11.3 μm requires the SiC dust.

For the alternative Model C, there are only C-rich dust shells that have similar superwind shells with the tenfold increase of the density but the disk parameters are the same as those for Model A. Model C, which produces a similar fit up to 20 μm, demonstrates that there would be no way to reproduce the water-ice emission features at 44 and 62 μm if there were no O-rich dust in the outer shells. Because β values of the O-rich dust shells are 31 times larger than those for C-rich dust shells, Model A produces more continuum radiation in the wavelength range 20–700 μm (see Figure 1), which assists in reproducing the overall observed SED.

6.4. Thin and Thick Disks of Silicate Dust

Figure 4 shows the polar contour diagrams of axisymmetric dust density distributions in the inner region ($r < 1200$ au). They show the thin ($h_0 = 0.01$) and thick ($h_0 = 0.1$) disks for Model A. The geometric thickness of the disk in the z direction is dependent on h_0, which is the ratio of the pressure scale height to the radius at R_0 (see Equation (7)).

The alternative Model D, which does not use the thin disk, produces a similar SED up to 100 μm but it does not reproduce the longer wavelength range. Very large silicate dust grains (S300) in the thin disk can reproduce the emission excesses in the FIR and mm wavelength bands fairly well. We expect that the size of dust grains in the long-lived thin disk can be very large by coagulation processes (see Section 3.1).

Note that the alternative Model B, which does not use the thick disk, produces emission features of crystalline silicates and water-ice. However, it does not produce enough radiation to reproduce the observed SED in the spectral range 8–70 μm. A thicker disk produces larger continuum emission in the wavelength range 8–70 μm. The thick disk of crystallized silicates (SFE50) can reproduce the conspicuous emission features of crystalline silicates in the wavelength range 8–45 μm of the *ISO* spectrum.

Different episodes of O-rich stellar winds (see Sections 3.3, 3.5, and 6.3) could have produced the two different disks: the long-lived thin disk and freshly formed thick disk. The thick disk of highly (~50%) crystallized silicates could have been formed recently by the superwind that produced the O-rich superwind shell (see Section 3.3). The superwind would be able to produce a thicker disk with a larger h_0 compared with the long-lived thin disk. There is observational evidence of thick disks for many post-AGB stars. Sahai et al. (2008) proposed that a massive dusty toroid is in the pre-planetary nebula IRAS 22036+5306. For the planetary nebulae the Red Rectangle and NGC 6302, the intensity distributions of the

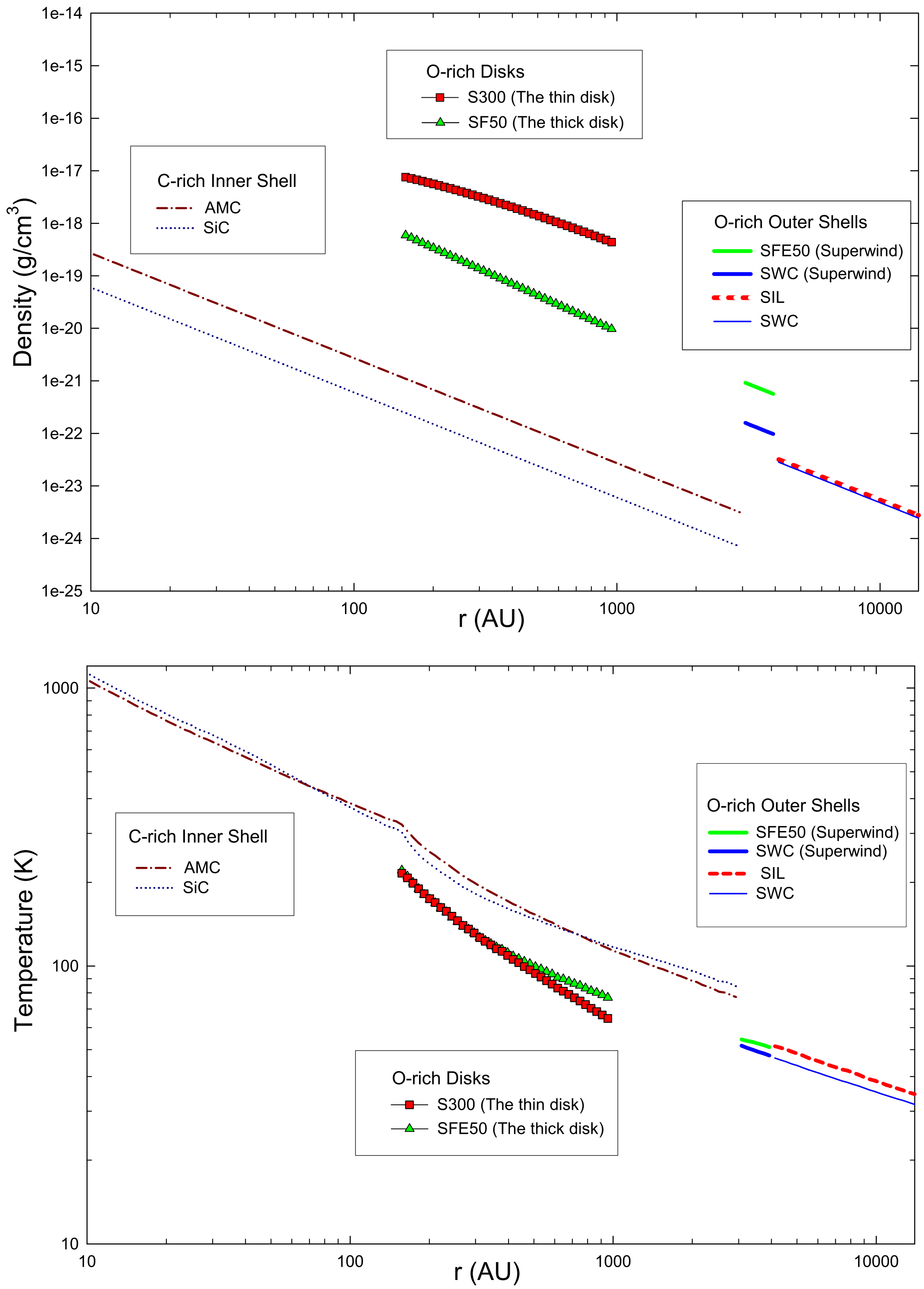

Figure 3. Dust density and temperature distributions for six shell components and two disk components in the direction of the disk plane ($z = 0$) for Model A (see Table 3 for detailed model parameters).

images imply a geometrically thick toruslike density distribution with bipolar conical cavities rather than a flat disk geometry (e.g., Men'shchikov et al. 2002; Peretto et al. 2007).

7. DISCUSSION

7.1. Implications of the Physical Model and Time Scales

The proposed physical model (see Section 3) for I09425, which is manifested by the best fit model presented in Section 6, may have some implications. We may estimate approximate timescales of the chemical transition processes from O to C using the model parameters for expanding dust shells. Because we assume that the constant expansion velocity ($V_{\rm exp}$) is $15 \pm 5\ {\rm km\ s^{-1}}$ (see Section 6.1) for all dust shells, every dust shell moves 1000 au in 320 ± 100 years.

For a long time prior to the chemical transition, which occurred 1300 ± 400 years ago, an O-rich AGB star had produced an O-rich dusty stellar wind. It produced the outermost O-rich dust shell ($r \approx$ 4000–15,000 au) and long-lived thin disk of large amorphous silicate grains (S300).

The superwind, which is induced by the last thermal pulse as an O-rich star in the chemical transition phase, began

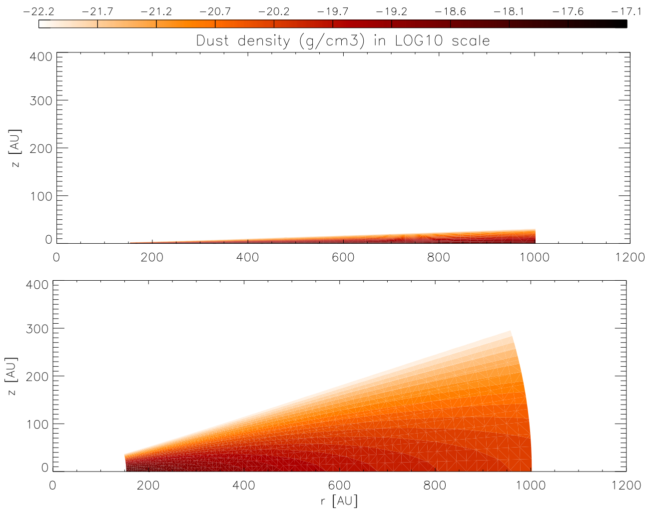

Figure 4. Axisymmetric dust density distributions of the O-rich dust disks for Model A. The thin ($h_0 = 0.01$) and thick ($h_0 = 0.1$) dust disks are shown.

1300 ± 400 years ago (corresponding to the shell radius $r \approx 4000$ au) and lasted for 320 ± 100 years (1000 au). It produced the O-rich superwind shell ($r \approx 3000$–4000 au) with highly (∼50%) crystallized silicate dust grains which are formed by high temperature annealing due to the superwind (see Section 3.3). The heavy stellar wind of highly crystallized silicate dust (SFE50) due to the superwind could produce the thick disk as well as the superwind shell.

In later phases, some SIL and SFE50 grains are coated with water-ice at colder temperatures to form the SWC in the outer expanding shells: the outermost ($r \approx 4000$–15,000 au; SIL, SWC) and superwind ($r \approx 3000$–4000 au; SFE50, SWC) shells.

The superwind ceased 960 ± 300 years ago ($r \approx 3000$ au) and the chemistry of the surface of the central star changed from O to C. The stellar wind from the carbon star began forming C-rich dust grains and produced the inner C-rich dust shell ($r \approx 10$–3000 au; AMC, SiC) which is still growing.

In 3800 ± 1000 years, all of the outer shell ($r \approx 10$–15,000 au) will be C-rich. However, we expect that silicate dust grains in the disks would remain with some changes for an extended time. A portion of the newly formed carbon dust could be added to the disks and the structures of the disks could be modified.

7.2. Water-ice in I09425

For high mass-loss rate OH/IR stars, Suh & Kwon (2013) found that SWC grains form at about 84–87 K in the expanding dust shells ($r \approx 1500$–1800 au). The dust disks for I09425 may not provide good conditions for forming water-ice mantles because the disks are located inside ($r \approx 150$–1000 au; $T_{\rm in,disk} > 200$ K) and more exposed to the stellar radiation for longer timescales.

For I09425, water-ice (SWC) in outer shells can reproduce the emission features at 44 and 62 μm. The water-ice contents (by mass) of the O-rich dust shells are 9.7% and 31% for the superwind and outermost shells, respectively. In the superwind shell ($r \approx 3000$–4000 au; SFE50, SWC; $T_c = 54$, 52 K), we expect that a relatively smaller content of SWC may form because the shell is more exposed to stellar radiation due to the lower dust density of the inner C-rich shell (see Section 6.3). The outermost shell ($r \approx 4000$–15,000 au; SIL, SWC; $T_c = 51$, 47 K) would be a better place for the formation of SWC because the thick inner superwind shell would effectively shield the stellar radiation (see Section 3.4).

The existence of both O-rich dust (water-ice) and C-rich dust in the expanding dust shells around I09425 would be strong evidence for the very recent chemical transition from O to C. I09425 could be a rare object that has the remnants of past O-rich stellar winds in the outer shells as well as in the disks.

7.3. Binary Stars and Dust Disks

There is some observational evidence for the presence of a disk in some silicate carbon stars. Ohnaka et al. (2008) made mid-IR interferometry observations toward BM Gem which suggested a circum-companion disk. For V778 Cyg, Szczerba et al. (2006) obtained high-resolution H_2O maser maps at 22 GHz and they concluded that the object is composed of a C-rich star and a companion that stores an O-rich disk. VLBA H_2O maser observations toward EU And also supported a circum-companion disk (Ohnaka & Boboltz 2008). These observations support the presence of an O-rich disk around a small-mass companion (a dwarf star).

The central star of the Red Rectangle (IRAS 06176-1036) is known as a spectroscopic binary with a period of 298 days (van Winckel et al. 1995). The companion star for the Red Rectangle is likely to be a main-sequence star (1–2 $M_\odot$; Men'shchikov et al. 2002). The object shows both PAH and crystalline silicate features. The Red Rectangle is a well known object that has a circum-binary disk that is viewed edge-on and that completely obscures the central binary (Cohen et al. 2004). The gas in the disk is known to rotate with Keplerian velocities and the gas disk contains about (2–6) $\times 10^{-3} M_\odot$ (Bujarrabal et al. 2005). Jura et al. (1997) detected low surface brightness radio emission at 2 cm and 1.3 cm that is extended well beyond $1''$ (∼670 au) from the source. They proposed that there is an orbiting, long-lived gravitationally bound disk of dust grains with very large radii.

We expect that most silicate carbon stars are likely to be binary systems rather than single stars. For I09425, the size (1000 ± 250 au) and total (gas and dust) mass ($(1.7 \pm 0.3) \times 10^{-2} M_\odot$) of the disk are comparatively large. This may mean that the disk is circum-binary rather than circum-companion and the mass of the companion star is comparatively large. Because the disk size and mass for I09425 are comparable to those of the Red Rectangle (see Men'shchikov et al. 2002), both objects could be binary systems with similar stellar parameters. I09425 looks like a predecessor to an object like the Red Rectangle in many respects.

7.4. Uncertainties

In Figure 1, the theoretical model reproduces quite well the observations in the whole spectral range except for the short wavelength part ($\lambda < 8\,\mu$m). The short wavelength part (2.4–8 μm) of the *ISO* SWS spectrum of I09425 is dominated by deep absorption bands produced by C-rich gas-phase molecules (CO, C_2, C_2H_2, and HCN) in the inner shells of the envelope (see Molster et al. 2001). The shorter wavelength range 1–2.4 μm, which is not observed by *ISO*, is also known to be dominated by the absorption bands of gas-phase molecules for a typical carbon star. In this work, we do not consider gas-phase molecules for the radiative transfer model

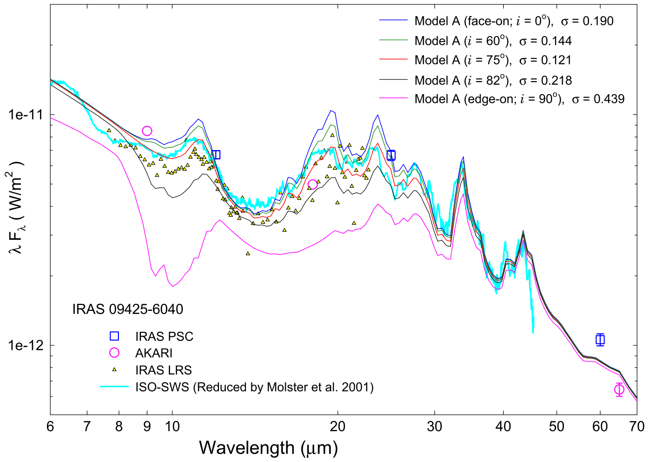

Figure 5. SED of I09425 compared with the model SEDs of the best fit model (Model A) for different viewing angles.

(see Section 4). Moreover, the observed fluxes may show some interstellar extinction in the wavelength range 1–2.4 μm.

Uncertainties remain in dust opacity. For crystalline silicate grains, the optical constants in a wide wavelength range are not known well and the opacity functions show wide variations depending on the dust sample and physical condition (e.g., Zeidler et al. 2015). The sizes of dust grains in different regions of the large dust envelope around a silicate carbon star could be too complicated to be considered by a simple scheme of Gaussian or power law distributions. The dust size could be very different depending on the physical and chemical condition of the region.

There is uncertainty in the viewing angle because the model SED is sensitively dependent on the viewing angle and there is no clue other than the observed SED. Figure 5 shows model SEDs of the best fit model (Model A) for different i. The model SED is sensitively dependent on i (for 0°–82°) only in the wavelength range 8–45 μm. The σ values were measured in the wavelength range 8–45 μm using the observational data from the *ISO* spectrum reduced by Molster et al. (2001). The model SED for $i = 75°$ shows the smallest σ value. Therefore, our choice of $i = 75°$ for all of the model SEDs displayed in Figure 1 could be justified because other model parameters can be constrained from the observations in other wavelength ranges.

7.5. Comparison with Previous Works

By using a spherically symmetric dust shell model, Molster et al. (2001) reproduced a similar SED in the wavelength range 20–45 μm for I09425. Because of the limitation of the model, they could not reproduce the observed SED in the wider wavelength range. The model did not reproduce the emission excess at 1.3 mm properly with the very large silicate dust grains (SIL300; see Section 5.2). For dust opacity, they used only O-rich dust species. Thus their model did not reproduce the SiC feature at 11.3 μm.

Molster et al. (2001) derived that the inner and outer radii are, respectively, $(1.3 \pm 0.1) \times 10^2$ and $(1.5 \pm 0.4) \times 10^4$ au for the O-rich dust shell. The outer radius is similar to our model result (see Section 6.1). The total dust mass was calculated to be $(1.5 \pm 0.3) \times 10^{-3}\,M_\odot$, which is larger than the one derived from this work ($(6.3 \pm 1) \times 10^{-4}\,M_\odot$). By using the large dust mass, their spherical dust shell model was not able to reproduce the similar SED in the FIR and mm bands for I09425.

Assuming that all dust grains are in a single geometrical component, Molster et al. (2001) proposed that crystalline silicates, which were crystallized as the result of a low-temperature crystallization process, are located in a long-lived disk. On the other hand, assuming that dust grains are in multiple shells and disks, we propose that crystalline silicates, which were formed through a high-temperature annealing process due to a superwind (see Sections 3.3, 3.5, 6.3, and 6.4), are in the outer shell and in the recently formed thick disk.

8. SUMMARY

I09425 is a silicate carbon star with conspicuous crystalline silicate and water-ice features and emission excess in the FIR and mm wavelength range. Based on the observations and known properties of AGB stars and dust species, we have proposed a physical model for I09425 using multiple dust shells and disks around a carbon star. We have performed model calculations for various possible combinations of dust shells and disks with different dust species to be compared with observations. We have compared the model results with the observed SEDs described by the *IRAS*, *ISO*, *AKARI*, and 2MASS data.

We have found that a theoretical model using multiple spherical shells of C-rich and O-rich dust and multiple disks of silicates around a carbon star can reproduce the observed SED of I09425 fairly well. The theoretical model has multiple dust shells that contain the total mass of $(4.6 \pm 0.9) \times 10^{-2}\,M_\odot$ for dust and gas and the outer radius is $(1.5 \pm 0.4) \times 10^4$ au. The mass-loss rates of the shells are $(2.2 \pm 1) \times 10^{-7} - (6.8 \pm 2) \times 10^{-5}\,M_\odot\,\mathrm{yr}^{-1}$. It also has large ($r = 1000 \pm 250$ au) O-rich disks with a total mass of $(1.7 \pm 0.3) \times 10^{-2}\,M_\odot$.

The model has detached O-rich dust shells and an inner C-rich dust shell. The innermost C-rich (AMC and SiC) dust shell reproduces the SiC feature at 11.3 μm. The detached cold (~50 K) O-rich (silicate and water-ice) dust shells could be remnants of the chemical transition from O to C. The inner O-rich dust shell of crystalline silicates with a tenfold density enhancement could have been formed by the superwind which is due to the last thermal pulse as an O-rich star in the chemical transition phase. The highly (~50%) crystallized silicate dust could be formed by high temperature annealing due to the superwind. The O-rich dust shells including the superwind shell produce water-ice and crystalline silicate features. They also produce more continuum radiation in the wavelength range 20–700 μm, which assists in reproducing the overall observed SED.

The theoretical model has a thin disk of large silicate grains and a thick disk of crystalline silicates. The large silicate dust grains in the long-lived thin disk can reproduce the emission excesses in the FIR and mm bands fairly well. The thick disk of crystallized silicates could have been formed recently by the superwind which produced the O-rich superwind shell. The freshly formed thick disk of crystallized silicates produces large continuum radiation in the wavelength range 8–70 μm and reproduces the conspicuous crystalline silicate emission features in the wavelength range 8–45 μm of the *ISO* spectrum.

The results of this paper support a scenario for the origin of silicate carbon stars where O-rich material was shed by mass-loss when the primary star was an M giant and this O-rich material was stored in a circumstellar disk. I09425 could be a rare object that has the remnants of past O-rich stellar winds in the outer shells as well as in the circum-binary disks.

I thank the anonymous referee for constructive comments and suggestions. This work was conducted during the research year of Chungbuk National University in 2015. This research was supported by the Basic Science Research Program through the National Research Foundation of Korea (NRF) funded by the Ministry of Science, ICT, & Future Planning (NRF-2013R1A1A2057841).

REFERENCES

Bertie, J. E., Labbé, H. J., & Whalley, E. 1969, JChPh, 50, 4501
Bjorkman, J. E., & Wood, K. 2001, ApJ, 554, 615
Bohren, C. F., & Huffman, D. R. 1983, Absorption and Scattering of Light by Small Particles (New York: Wiley)
Bujarrabal, V., Castro-Carrizo, A., Alcolea, J., & Neri, R. 2005, A&A, 441, 1031
Chan, S. J., & Kwok, S. 1990, A&A, 237, 354
Chan, S. J., & Kwok, S. 1991, ApJ, 383, 837
Chen, P. S., Yang, X.-H., & Zhang, P. 2007, AJ, 134, 214
Chihara, H., Koike, C., Tsuchiyama, A., Tachibana, S., & Sakamoto, D. 2002, A&A, 391, 267
Cohen, M., Van Winckel, H., Bond, H. E., & Gull, T. R. 2004, AJ, 127, 2362
Cutri, R. M., Skrutskie, M. F., van Dyk, S., et al. 2003, yCat, 2246, 0
Fabian, D., Jäger, C., Henning, Th., Dorschner, J., & Mutschke, H. 2000, A&A, 364, 282
Galt, J. A., Kwok, S., & Frankow, J. 1989, AJ, 98, 2182
García-Hernández, D. A., Abia, C., Manchado, A., & García-Lario, P. 2006, A&A, 452, 1049
García-Lario, P., Manchado, A., Pych, W., & Pottasch, S. R. 1997, A&AS, 126, 479
Groenewegen, M. A. T., van den Hoek, L. B., & de Jong, T. 1995, A&A, 293, 381
Iben, I., & Renzini, A. 1983, ARA&A, 21, 271
Iben, I., Jr. 1981, ApJ, 246, 278
Jäger, C., Molster, F. J., Dorschner, J., et al. 1998, A&A, 339, 904
Jiang, B. W., Deguchi, S., Yamamura, I., et al. 1996, ApJS, 106, 463
Jones, T. W., & Merrill, K. M. 1976, ApJ, 209, 509
Juhász, A., Henning, Th., Bouwman, J., et al. 2009, ApJ, 695, 1024
Jura, M., Turner, J., & Balm, S. P. 1997, ApJ, 474, 741
Justtanont, K., Olofsson, G., Dijkstra, C., & Meyer, A. W. 2006, A&A, 450, 1051
Kenyon, S. J., & Hartmann, L. 1987, ApJ, 323, 714
Koike, C., Chihara, H., Tsuchiyama, A., et al. 2003, A&A, 399, 1101
Kozasa, T., Hasegawa, H., & Seki, J. 1984, Ap&SS, 98, 61
Kwon, Y.-J., & Suh, K.-W. 2014, JKAS, 47, 123
Lagadec, E., Sloan, G. C., Zijlstra, A. A., Mauron, N., & Houck, J. R. 2012, MNRAS, 477, 2588
Little-Marenin, I. R. 1986, ApJ, 307, 15
Lloyd Evans, T. 1990, MNRAS, 243, 336
Loup, C., Forveille, T., Omont, A., & Paul, J. F. 1993, A&AS, 99, 291
Men'shchikov, A. B., Schertl, D., Tuthill, P. G., Weigelt, G., & Yungelson, L. R. 2002, A&A, 393, 867
Molster, F. J., Yamamura, I., Waters, L. B. F. M., et al. 2001, A&A, 366, 923
Morris, M. 1987, PASP, 99, 1115
Murakami, H., Baba, H., Barthel, P., et al. 2007, PASJ, 59, S369
Ohnaka, K., & Boboltz, D. A. 2008, A&A, 478, 809
Ohnaka, K., Izumiura, H., Leinert, C., et al. 2008, A&A, 490, 173
Pégourié, B. 1988, A&A, 194, 335
Peretto, N., Fuller, G., Zijlstra, A., & Patel, N. 2007, A&A, 473, 207
Sahai, R., Young, K., Patel, N., Sánchez Contreras, C., & Morris, M. 2008, Ap&SS, 313, 241
Sauter, J., & Wolf, S. 2011, A&A, 527, 27
Suh, K.-W. 1997, MNRAS, 289, 559
Suh, K.-W. 1999, MNRAS, 304, 389
Suh, K.-W. 2000, MNRAS, 315, 740
Suh, K.-W. 2002, MNRAS, 332, 513
Suh, K.-W. 2004, ApJ, 615, 485
Suh, K.-W. 2014, JKAS, 47, 219
Suh, K.-W., Jones, T. J., & Bowen, G. H. 1990, ApJ, 358, 588
Suh, K.-W., & Kwon, Y.-J. 2013, ApJ, 762, 113
Szczerba, R., Szymczak, M., Babkovskaia, N., et al. 2006, A&A, 452, 561
van Winckel, H., Waelkens, C., & Waters, L. B. F. M. 1995, A&A, 293, L25
Vassiliadis, E., & Wood, P. R. 1993, ApJ, 413, 641
Willems, F. J., & de Jong, T. 1986, ApJ, 309, 39
Wolf, S., & Voshchinnikov, N. V. 2004, CoPhC, 162, 113
Wood, P. R. 1990, in From Miras to Planetary Nebulae: Which Path Evolution, ed. M. O. Minnessier, & A. Omont (Gif sur Yvette: Editions Frontiéres), 67
Yamamura, I., Dominik, C., de Jong, T., Waters, L. B. F. M., & Molster, F. J. 2000, A&A, 363, 629
Zeidler, S., Mutschke, H., & Posch, Th. 2015, ApJ, 798, 125
Zuckerman, B., & Lo, K. Y. 1987, A&A, 173, 263